Title

CH4 sources estimated from atmospheric observations of CH4 and its C-13/C-12 isotopic ratios: 2. Inverse modeling of CH4 fluxes from geographical regions

Journal

Global Biogeochemical Cycles, 18(4)

ISSN

0886-6236

Authors

Mikaloff Fletcher, S.E.
Tans, P P
Bruhwiler, L M
et al.

Publication Date

2004-10-01

Peer reviewed

CH_4 sources estimated from atmospheric observations of CH_4 and its $^{13}C/^{12}C$ isotopic ratios: 2. Inverse modeling of CH_4 fluxes from geographical regions

Sara E. Mikaloff Fletcher[1]
Cooperative Institute for Research in Environmental Science (CIRES), University of Colorado, Boulder, Colorado, USA

Pieter P. Tans, Lori M. Bruhwiler, and John B. Miller
National Oceanic and Atmospheric Administration Climate Modeling Diagnostics Laboratory (NOAA CMDL), Boulder, Colorado, USA

Martin Heimann
Max-Planck-Institut Für Biogeochemie, Jena, Germany

Received 14 January 2004; revised 14 June 2004; accepted 24 July 2004; published XX Month 2004.

[1] We present a time-dependent inverse modeling approach to estimate the magnitude of CH_4 emissions and the average isotopic signature of the combined source processes from geographical regions based on the observed spatiotemporal distribution of CH_4 and $^{13}C/^{12}C$ isotopic ratios in CH_4. The inverse estimates of the isotopic signature of the sources are used to partition the regional source estimates into three groups of source processes based on their isotopic signatures. Compared with bottom-up estimates, the inverse estimates call for larger CH_4 fluxes in the tropics (266 ± 25 Tg CH_4/yr) and southern extratropics (98 ± 15 Tg CH_4/yr) and reduced fluxes in the northern extratropics (252 ± 18 Tg CH_4/yr). The observations of $^{13}C/^{12}C$ isotopic ratios in CH_4 indicate that the large a posteriori CH_4 source in the tropics and Southern Hemisphere is attributable to a combination both bacterial sources and biomass burning and support relatively low estimates of fossil CH_4 emissions. *INDEX TERMS:* 0315 Atmospheric Composition and Structure: Biosphere/atmosphere interactions; 0322 Atmospheric Composition and Structure: Constituent sources and sinks; 0368 Atmospheric Composition and Structure: Troposphere—constituent transport and chemistry; 1040 Geochemistry: Isotopic composition/chemistry; *KEYWORDS:* $^{13}C/^{12}C$ isotopic ratios, inverse modeling, methane sources

Citation: Mikaloff Fletcher, S. E., P. P. Tans, L. M. Bruhwiler, J. B. Miller, and M. Heimann (2004), CH_4 sources estimated from atmospheric observations of CH_4 and its $^{13}C/^{12}C$ isotopic ratios: 2. Inverse modeling of CH_4 fluxes from geographical regions, *Global Biogeochem. Cycles*, *18*, GBXXXX, doi:10.1029/2004GB002224.

1. Introduction

[2] Atmospheric CH_4 plays a major role in Earth's radiative budget and atmospheric chemistry. CH_4 contributes about 20% of the total radiative forcing from long-lived greenhouse gases. CH_4 is also an important sink for OH radical, the major determinant of the oxidizing capacity of Earth's atmosphere, affects O_3 chemistry in the troposphere and the stratosphere, and leads to the production of stratospheric water vapor. The CH_4 mixing ratio in the atmosphere has increased by 150% since pre-industrial times, and based on the ice core record of atmospheric CH_4, current levels of CH_4 have not been exceeded for the last 420,000 years [*Petit et al.*, 1999].

[3] A great deal of progress has been made toward estimating the sources and sinks of CH_4 through models of the source processes and combining local observations of CH_4 emissions or emission ratios with land use inventories, energy use or agricultural data, or other relevant statistical information [e.g., *Matthews and Fung*, 1987; *Aselmann and Crutzen*, 1989; *Olivier et al.*, 1996; *Levine et al.*, 2000; *Kaplan*, 2001]. However, owing to the large spatial and temporal variability of many of the source processes, these estimates are associated with a great deal of uncertainty. Forward model simulations which determine the atmospheric spatiotemporal distribution of CH_4 based on estimates of the sources and sinks have found that these bottom-up estimates lead to an overestimate of the interhemispheric gradient relative to the atmospheric observations [e.g., *Fung et al.*, 1991; *Hein et al.*, 1997; *Houweling et al.*, 1999] (Figure 1), suggesting our process-level understanding of the CH_4 cycle is incomplete. In addition, bottom-up estimates often do not account for interannual

[1]Now at the Department of Atmospheric and Oceanic Sciences, University of California, Los Angeles, California, USA.

0886-6236/04/2004GB002224$12.00

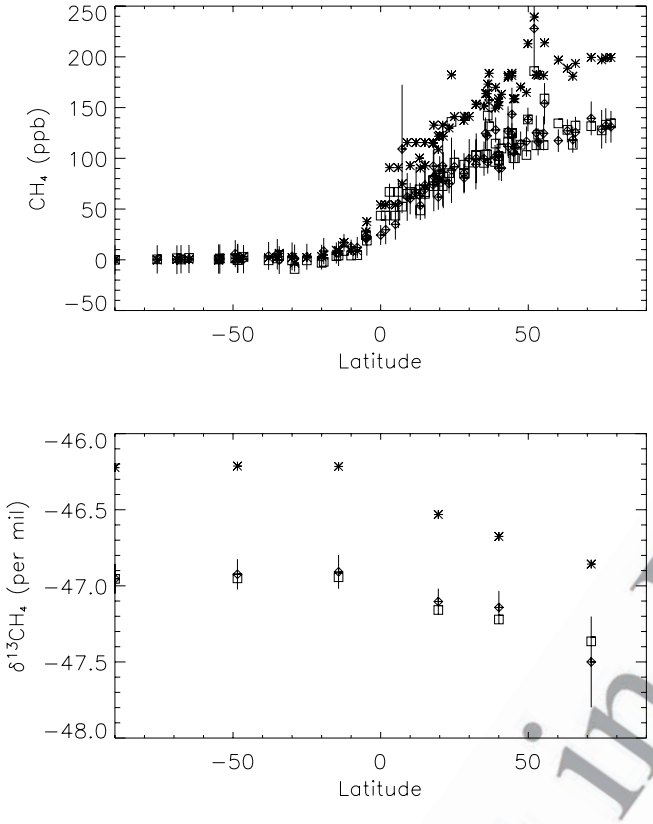

Figure 1. Latitudinal gradient of (top) CH_4 and (bottom) $\delta^{13}CH_4$ of the observations (diamonds), forward simulation based on the a priori estimates (asterisks), and forward simulation based on the a posteriori source estimates (squares). Error bars on the observations reflect the standard deviation of the individual observations from the annual mean.

variability of the CH_4 sources. Owing to the variability of the CH_4 growth rate [*Dlugokencky et al.*, 2003, 2001], methods that elucidate the causes for interannual variability in the CH_4 cycle are highly desirable.

[4] Inverse modeling has also been used to optimize CH_4 fluxes based on observations of the atmospheric CH_4 mixing ratios and a model of atmospheric transport [e.g., *Hein et al.*, 1997; *Houweling et al.*, 1999; *Bergamaschi et al.*, 2000; *Chen*, 2004]. Several inverse studies have used an estimate of the spatial footprint for each source process, the observations of CH_4, and, in some cases, its $^{13}C/^{12}C$ isotopic ratios to estimate the global source strength of each source process [*Hein et al.*, 1997; *Bergamaschi et al.*, 2000; *Mikaloff Fletcher et al.*, 2004]. This approach is subject to considerable uncertainty due to the inherent assumption that the a priori spatial pattern of the source processes is perfect and does not vary interannually. Inverse methods have been used to optimally estimate, within certain assumptions, the spatial pattern of the CH_4 flux required by the CH_4 observations [*Houweling et al.*, 1999], without first partitioning the sources into source processes with their own spatial patterns. However, owing to the spatial overlap of the source processes, this approach does not elucidate the underlying causes for changes in the CH_4 flux estimates.

[5] The observed $CH_4^{13}C/^{12}C$ isotopic ratio has also been used to constraint the CH_4 budget [e.g., *Miller et al.*, 2002; *Quay et al.*, 1999; *Mikaloff Fletcher et al.*, 2004] due to the differing isotopic signatures of different source processes (Table 1). The $^{13}C/^{12}C$ isotopic ratio, R_{sample}, is often expressed as a deviation from an arbitrary standard, $R_{\text{reference}}$, in order to accentuate the very small changes in atmospheric $^{13}C/^{12}C$ due to the isotopic signatures of the sources.

$$\delta^{13}C = \left(\frac{R_{\text{sample}}}{R_{\text{reference}}} - 1\right) \times 1000, \quad (1)$$

In this case, $R_{\text{reference}}$ is the Peedee Belemite carbonate standard [*Craig*, 1953]. Methane generated by bacteria in anaerobic environments including wetlands, rice paddies, and the digestive tracts of ruminant animals and termites is more depleted in ^{13}C than the background atmosphere, methane emitted from biomass burning is less depleted in ^{13}C than the background atmosphere, and CH_4 from fossil fuels such as coal and natural gas is relatively close to the atmospheric $\delta^{13}C$ signature. While landfill CH_4 emissions are generated by anaerobic bacteria, the isotopic signature of landfill CH_4 is less depleted in ^{13}C than the other bacterial sources due to partial oxidation of CH_4 within the landfill.

Table 1. A Priori CH_4 Source Estimates and the Mean $\delta^{13}CH_4$ Isotopic Signatures of the Sources and Sinks

	A Priori Estimates, Tg CH_4/yr	Mean Isotopic Signature
Sources		
Bacterial sources		
Swamps	91[a]	−58‰[b]
Bogs and tundra	54[a]	−58‰[b]
Rice agriculture	60[c]	−63‰[b]
Ruminant animals	93[c]	−60‰[b]
Termites	20[d]	−70‰[b]
Biomass burning	52[e]	−25‰[b]
Fossil Fuels		
Coal	38[c]	−37‰[b]
Natural gas and other industrial	57[c]	−44‰[b]
Landfills	50[f]	−55‰[b]
Prescribed Sources and Sinks		
Hydrates	10[g]	−60‰[b]
Ocean	5[g]	−60‰[b]
Tropospheric OH	507[h]	5.4‰[i]
Stratospheric loss	40[j]	12‰[k]
Soils	30[j]	22‰[l]

[a] *Lelieveld et al.* [1998].
[b] *Whiticar* [1993].
[c] EDGAR emissions database [*Olivier et al.*, 1996].
[d] *Sanderson* [1996].
[e] *Levine et al.* [2000].
[f] *Bingemer and Crutzen* [1987].
[g] *Cicerone and Oremland* [1988].
[h] On the basis of *Spivakovsky et al.* [2000] OH fields and model CH_4 mixing ratios, tuned to *IPCC* [2001] total CH_4 loss.
[i] *Cantrell et al.* [1990].
[j] *IPCC* [2001].
[k] *Brenninkmeijer et al.* [1995], reflecting the total observed isotopic fractionation due to OH, O^1D, and Cl in the stratosphere.
[l] *Tyler et al.* [1994].

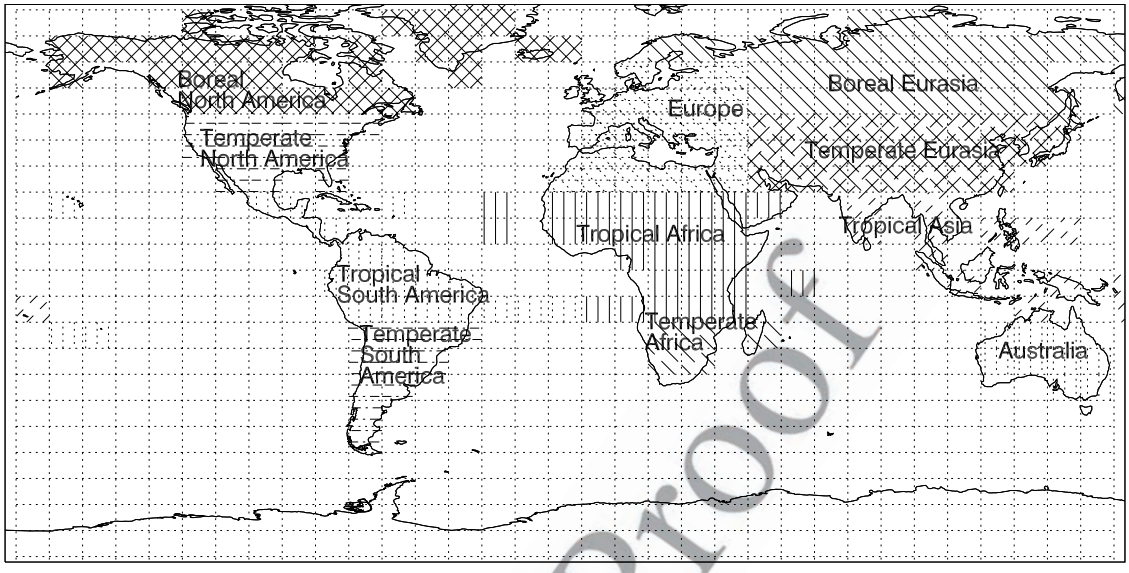

Figure 2. The eleven spatial land region definitions used in the inverse model.

[6] In this work, we demonstrate a novel approach to partition regional inverse estimates of CH_4 into three broad categories of source processes based on the atmospheric observations of $\delta^{13}CH_4$. We present time-dependent CH_4 fluxes from 11 geographical regions and inverse estimates of the $\delta^{13}CH_4$ isotopic signature from all source processes from three latitude bands for 1998–1999. The a posteriori isotopic signatures of the sources are used to determine the contributions of the bacterial, biomass burning and fossil fuel source processes to the a posteriori CH_4 fluxes and discuss the likely physical causes for differences between bottom-up source estimates and the inverse estimates. Changes in the annual mean fluxes for 1998–1999 are discussed in the context of the 1998 growth rate anomaly. Finally, the sensitivity of the inverse estimates is tested with respect to changes in several model parameters.

2. Methods

[7] The experimental design in this work is described in detail by *Mikaloff Fletcher et al.* [2004]. Here we provide a brief overview of the model setup, then focus on the differences between these two studies.

[8] The model transport is represented by the coarse grid version of Tracer Model 3 (TM3) [*Heimann and Körner*, 2003] with a resolution of 7.8° latitude by 10° longitude by nine vertical levels. TM3 was driven by The National Centers for Weather Prediction/National Center for Atmospheric Research (NCEP/NCAR) wind fields corresponding to the year being modeled. The model was initialized using three-dimensional CH_4 and $\delta^{13}CH_4$ fields from the final time step of a "test" inversion which was initialized using observed hemispheric mean values [*Miller et al.*, 2002]. The first 3 months of the final inverse results were excluded to minimize inaccuracies due to initial conditions. The CH_4 sinks were prescribed as described by *Mikaloff Fletcher et al.* [2004].

[9] *Mikaloff Fletcher et al.* [2004] estimated the global total source strength for each source process. This allows the isotopic fractionation of each source to be prescribed in order to use the isotopic ratios measured at each observing station as additional constraints on the methane flux estimates. In this study, the world is divided into 11 geographical regions (Figure 2), and CH_4 flux is estimated for each spatial region based on the GLOBALVIEW-CH_4 [*National Oceanic and Atmospheric Administration* (*NOAA*), 2001] data set and a priori estimates of the sources (Table 1). Since the emissions within a spatial region are typically due to many source processes whose relative contributions are poorly known, the isotopic signatures of the net source from each model region is calculated using the inverse model constrained by observations of the isotopic signature at six observing stations from the NOAA/CMDL network shown in Table 2 [*Miller et al.*, 2002] and a priori estimates based on the flux estimates and isotopic signatures in Table 1. These isotopic signatures are then used as an additional constraint on the total CH_4 flux and to partition the regional fluxes between source processes. Only six observing stations with measurements of $\delta^{13}CH_4$ were included in this work, so the inverse model will not be able to constrain all 11 model regions for $\delta^{13}CH_4$. Thus, for the inversion for

Table 2. NOAA/CMDL Cooperative Air Sampling Network Sites With $\delta^{13}CH_4$ Observations

Name	Site Code	Location	Elevation, m
Barrow, Alaska, USA	BRW	71°19′N 156°36′W	11
Niwot Ridge, Colorado, USA	NWR	40°03′N 105°35′W	3475
Mauna Loa, Hawaii, USA	MLO	19°32′N 155°35′W	3397
Cape Matatula, American Samoa	SMO	14°15′S 170°34′W	42
Cape Grim, Tasmania	CGO	40°41′S 144°41′E	94
South Pole, Antarctica	SPO	89°59′S 24°48′W	2810

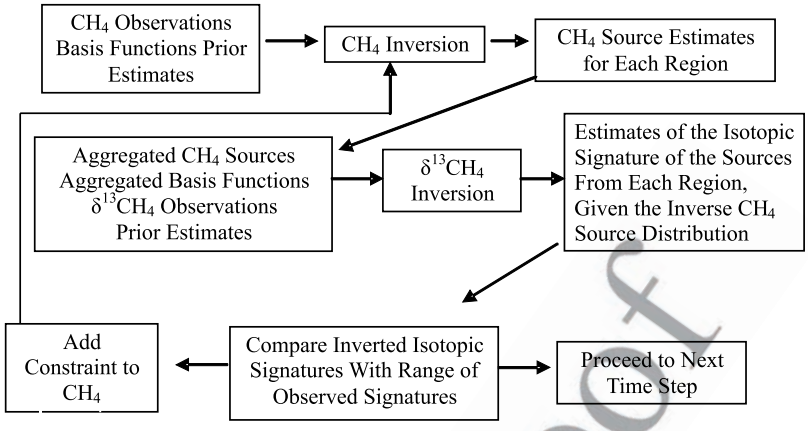

Figure 3. Schematic description of the iterative process used to estimate CH_4 sources and $\delta^{13}CH_4$.

the isotopic signatures, these regions are aggregated to three latitude bands: north of 23.5°N, 23.5°N to 15.7°S, and south of 15.7°S.

[10] Although there are long-term observational records of $\delta^{13}CH_4$ at a number of observing stations [e.g., *Lowe et al.*, 1994; *Quay et al.*, 1999; *Bergamaschi et al.*, 2000], only the observations from the NOAA/CMDL network were included in the inverse model. *Miller et al.* [2002] demonstrated that there may be offsets between laboratories of about 0.1‰, which could lead to significant biases in the inverse model. This highlights the need for $\delta^{13}CH_4$ measurement intercomparisons.

[11] Like *Mikaloff Fletcher et al.* [2004], monthly fluxes for 1998–2000 were estimated using a time-dependent mass balance inversion [*Bruhwiler et al.*, 2000]. The difference between the observed mixing ratio of a trace gas at the jth station, y_j^{obs}, and the model simulated mixing ratio in the absence of sources, y_j, is treated as the sum over nreg discrete model regions of the source strengths, x_i, multiplied by basis functions, $H_{i,j}$, which represent the atmospheric response at the jth station to an arbitrary unit flux from the ith region.

$$y_j^{\text{obs}} - y_j = \sum_{i=1,\text{nreg}} \mathbf{H}_{i,j} x_i. \tag{2}$$

The modeled mixing ratio, y_j^{obs}, is calculated by applying the transport model to the three-dimensional tracer field from the previous month. The basis function for a given region and a given month is simulated by emitting a steady flux from the region, distributed spatially within the region according to an a priori estimate of the sources, and allowing the transport model to act on these emissions. Then, the modeled three-dimensional mixing ratio field is sampled at the station locations at the end of the month.

[12] In order to estimate the isotopic signature of the sources, equation (2) can be rewritten in terms of the mixing ratio ^{13}C and the $^{13}C/^{12}C$ isotopic ratio of the sources from each region, R_i, as follows:

$$y_{j_{13C}}^{\text{obs}} - y_{j_{13C}} = \sum_{\text{nreg}} H_{i,j} x_i R_i. \tag{3}$$

By dividing equation (3) by $R_{\text{reference}}$, then subtracting equation (2), the following expression can be written

$$\frac{y_{j_{13C}}^{\text{obs}} - y_{j_{13C}}}{R_{\text{reference}}} - \left(y^{\text{obs}} - y\right) = \sum_{\text{nsrc}} H_{i,j} x_i \left(\frac{R_i}{R_{\text{reference}}} - 1\right). \tag{4}$$

Dividing equation (4) by equation (2) and multiplying by 1000, this equation begins to take on the form of δ units (equation (1)), which are needed to emphasize the small differences in $^{13}C/^{12}C$ ratios caused by the isotopic signatures of the sources.

$$\left(\frac{y_{j_{13C}}^{\text{obs}} - y_{j_{13C}}}{\left(y_j^{\text{obs}} - y_j\right) R_{\text{std}}} - 1\right) \times 1000 = \frac{\sum_{\text{nsrc}} H_{i,j} x_i \delta_i}{\sum_{\text{nsrc}} H_{i,j} x_i}. \tag{5}$$

The left-hand side of equation (5) is the "effective" δ value of the net difference between observed and simulated mixing ratios, which is defined here as δ_{diff}

$$\delta^{\text{diff}} = \left[\frac{y_{j_{13C}}^{\text{obs}} - y_{j_{13C}}}{\left(y_j^{\text{obs}} - y_j\right) R_{\text{std}}} - 1\right] \times 1000. \tag{6}$$

For a small fraction of data points, the difference $y_{j_{13C}}^{\text{obs}} - y_{j_{13C}}$ is very close to zero, which leads to spurious values of δ^{diff}. These data are excluded from the inversion. In the inverse model, this difference represents the total signal of the sources at the station over a given month (equation (3)); therefore, these data points are not likely to provide a strong constraint to the inverse model.

[13] Note that equation (5) contains nonlinearity, as it is dependent on x_i and δ, both of which are variable in the inverse model. An iterative approach is used to deal with this problem, shown schematically in Figure 3. First, equation (2) is solved for the CH_4 sources. Then, the basis functions and sources are aggregated to the larger $\delta^{13}CH_4$ source regions, and equation (5) is solved for the isotopic signature of the sources holding the sources fixed. The calculated isotopic signatures from each source region can be used both qualitatively and quantitatively as an interpretive tool to partition the fluxes within spatial regions

t3.1 **Table 3.** Summary of the Inversion Scenarios Implemented to Compare Prior Estimates With Inverse Results and Test the Sensitivity of the Inverse Results to Various Sources of Error

t3.2 Scenario	Description	Additional Details
t3.3 S0	a priori source estimates	forward simulation of prior source estimates shown in Table 1.
t3.4 S1	a posteriori estimates, including observations of $\delta^{13}CH_4$	inverse source estimates
t3.5 S2	sensitivity to OH kinetic isotope effect	S1 with the *Saueressig et al.* [2001] measurement of the KIE for OH
S3	sensitivity to OH fields- Upper limit	S1 with OH increased by 15% to the upper end of the uncertainty
t3.6		estimate of *Spivakovsky et al.* [2000]
S4	sensitivity to OH fields- Lower limit	S1 with OH decreased 15% to the lower end of the uncertainty
t3.7		estimate of *Spivakovsky et al.* [2000]
S5	sensitivity to initial conditions	S1 initialized to the observed hemispheric mean CH_4 and $\delta^{13}CH_4$
t3.8		for 1998 [*Miller et al.*, 2002]

between source processes. Finally, the inverse isotopic signatures are compared to the range of observed isotopic signatures of the source processes (Table 1) and in some cases used to constrain the CH_4 estimates.

[14] In the absence of error, the a posteriori isotopic signature for a given latitude band could only match the high or low end of this range of isotopic signatures if the CH_4 flux from the latitude band were composed almost entirely of either biomass burning or bacterial sources. At a few model time steps, the estimated isotopic signature exceeds the range of isotopic signatures of the source processes. There is considerable uncertainty associated with the isotopic signatures of the source processes. However, an a posteriori isotopic signature of this magnitude would require both a significant excursion from the observed isotopic signature of the source processes and the unlikely source scenario mentioned above. Therefore it seems reasonable to assume in these cases that there may be an error in the inverse estimate of CH_4.

[15] When the a posteriori isotopic signatures are greater than −25‰ or less than −65‰, a feedback mechanism is activated to constrain the CH_4 flux estimates using the isotope data. This constraint is formulated by re-arranging equation (5) and replacing the a posteriori estimate of δ_i for the regions with spurious isotopic signature estimates with either the minimum or maximum in the range of signatures from the source processes, $\delta_{min/max}$.

$$\delta_{diff} \sum_{nsrc} H_{i,j} x_i = \sum_{nsrc} H_{i,j} x_i \delta_{min/max}. \quad (7)$$

[16] The total effect of the sources, $\sum_{nsrc} H_{i,j} x_i$, is treated as a constant, since this quantity is equal to the difference $y_j^{obs} - y_j$. This is repeated iteratively until the criteria of a match to the station observations of CH_4, $\delta^{13}CH_4$, and the range of reasonable isotopic signatures are all matched. While we correct the CH_4 flux estimates with the isotopic data in these cases where the presence of an error is clear, one important weakness of this technique is that any error associated with the CH_4 source estimates is propagated to the $\delta^{13}CH_4$ estimates.

[17] The a priori CH_4 flux estimates and spatial patterns for these land regions were calculated by distributing the a priori source process estimates (Table 1) spatially according the NASA Goddard Institute for Space Studies (GISS) flux maps [*Fung et al.*, 1991], and the uncertainties assigned to the prior estimates are based on the range of estimates given by the *IPCC* [2001], as per *Mikaloff Fletcher et al.* [2004]. Similarly, the a priori $\delta^{13}C$ isotopic signatures are based on a flux-weighted average of the isotopic signatures shown in Table 1 for each region. An uncertainty of 0.15‰ was assigned to the prior estimates. This value was selected based on equilibrium estimates of how much relatively large changes in the fluxes or the isotopic signatures of the sources might change the a priori isotopic signature on large spatial scales. For example, a shift of 100 Tg of CH_4 from wetlands to biomass burning would result in a change in the global isotopic signature of about 0.15‰ based on a global total source of 550 Tg CH_4/yr, and a change in the global wetland isotopic signature of 0.13‰ based on the source estimates of *Mikaloff Fletcher et al.* [2004]. The relatively large uncertainty estimates associated with the priors were chosen to allow a strongly data-driven inversion. The uncertainties assigned to the CH_4 observations were based on the mean standard deviation of the observations from the smoothed curve, as described by *Mikaloff Fletcher et al.* [2004]. The uncertainty associated with the calculated δ_{diff}, σ_{diff}, is calculated using mean values of the differences $y_j^{obs} - y_j$ and $y_{j_{13C}}^{obs} - y_{j_{13C}}$ and the uncertainties for these two differences, σ_{CH4} and σ_{C13}.

$$\sigma_{diff} = \sqrt{\left(\frac{\sigma_{CH4}\left(y_{j_{13C}}^{obs} - y_{j_{13C}}\right)}{R_{std}}\right)^2 + \left(\frac{\sigma_{CH4}}{\left(y_j^{obs} - y_j\right)R_{std}}\right)^2}. \quad (8)$$

Like σ_{CH4}, σ_{C13} is calculated based on the mean standard deviation of the observations from the smoothed curve. Finally, for cases in which the isotopes are used to constrain the CH_4 flux estimates using equation (6), σ_{const}, the uncertainty associated with this constraint is represented by

$$\sigma_{const} = \sqrt{\left(\sigma_{\Sigma Hx} \times \delta_{diff}\right)^2 + \left(\sigma_{diff} \sum_{nsrc} H_{i,j} x_i\right)^2}, \quad (9)$$

where the uncertainty associated with the sum of the methane sources multiplied by the basis functions, $\sigma_{\Sigma Hx}$ was taken to be 20% of the value of the total.

[18] In section 7, the sensitivity of the inverse technique to several potential sources of error is tested using the scenarios summarized in Table 3.

3. Inverse CH_4 Estimates

[19] Overall, the a posteriori sources in the Northern Hemisphere (NH) are decreased relative to a priori esti-

t4.1 **Table 4.** Time-Averaged CH_4 Source Estimates for the A Priori Fluxes (S0), and the A Posteriori Estimates for Several Inverse Scenarios Described in Table 1[a]

t4.2 Model Region	S0	S1	S2	S3	S4	S5
t4.3 Boreal North America	21 ± 16	16 ± 4	13 ± 5	13 ± 5	15 ± 4	21 ± 4
t4.4 Boreal Eurasia	43 ± 28	15 ± 8	23 ± 8	24 ± 9	15 ± 8	9 ± 8
t4.5 Temperate North America	58 ± 13	54 ± 8	56 ± 9	59 ± 9	45 ± 8	46 ± 8
t4.6 Europe	69 ± 15	69 ± 8	64 ± 8	66 ± 8	65 ± 8	72 ± 8
t4.7 Temperate Eurasia	98 ± 42	98 ± 11	103 ± 11	106 ± 11	86 ± 11	88 ± 11
t4.8 Tropical South America	53 ± 25	73 ± 16	77 ± 17	87 ± 17	44 ± 15	62 ± 15
t4.9 Northern Africa	47 ± 21	80 ± 17	73 ± 17	79 ± 17	63 ± 17	86 ± 17
t4.10 Tropical Asia	76 ± 38	113 ± 10	112 ± 10	119 ± 10	93 ± 9	114 ± 10
t4.11 Southern Africa	9 ± 3	10 ± 2	10 ± 2	10 ± 2	9 ± 2	10 ± 2
t4.12 Temperate South America	36 ± 20	71 ± 14	73 ± 15	81 ± 15	50 ± 13	70 ± 13
t4.13 Australia	13 ± 4	17 ± 4	19 ± 4	20 ± 4	15 ± 4	16 ± 3
t4.14 **Global**	**523 ± 78**	**618 ± 28**	**624 ± 29**	**662 ± 30**	**498 ± 28**	**592 ± 28**

t4.15 [a]Note that the relatively small ocean sources and all of the CH_4 sinks have been prescribed.

mates, while sources in the Southern Hemisphere (SH) are increased relative to the prior estimates (Table 4, Figure 4), a robust result that is in general agreement with the forward results (Figure 1) and previous inverse studies [i.e., *Mikaloff Fletcher et al.*, 2004; *Houweling et al.*, 1999; *Hein et al.*, 1997; *Chen*, 2004]. The bulk of this reduction occurs in boreal Eurasia, with a smaller reduction in boreal North America. These high northern latitude regions are well sampled by the observing network and well constrained by the CH_4 observations, given the a priori detailed spatial patterns. The observations also call for smaller emissions from temperate North America than the prior estimates, but this difference is much smaller than the error limits estimated by the inverse model. The inverse model estimates the largest increases over the a priori estimates in the tropical regions of South America, Africa, and Asia. There are also significant increases in emissions from temperate South America. This region coincides with a major region of wetlands in the SH [*Kaplan*, 2001; *Walter*, 1998]. However, owing to the paucity of CH_4 observations that constrain these regions, the partitioning between temperate South America, Southern Africa, and Australia may not be robustly driven by the observations. In addition, the observational constraints lead to reductions in the uncertainties associated wit the a priori estimates, especially for regions in the NH.

[20] The two-dimensional spatial distribution of CH_4 flux that would result from these regional source estimates has been illustrated by distributing the regional fluxes according to the spatial patterns used for the basis functions (Figure 3). As discussed above, the overall interhemispheric gradient and many continental scale features are similar between this approach and a source process inversion [*Mikaloff Fletcher et al.*, 2004]. For example, both approaches call for large flux increases over tropical South America and Central Africa compared to the a priori estimates and large decreases in North America and Europe. This shows that these broad results are robust with respect to different definitions of the model regions and different approaches to the application of the isotopes to constrain the CH_4 flux. However, the regional details are distinctly different. The source process approach attributed much of the decrease in NH sources to fossil fuels and landfills; therefore the greatest a posteriori decreases occur in the industrial regions of the United States and Europe. Conversely, the regional inversion assigns the largest decreases to high northern latitude regions, especially boreal Eurasia which would be more likely to be associated with emissions from boreal wetlands. In section 4, the ^{13}C isotopic signatures will be used to determine which source process is most consistent with the observations.

[21] It is worthy of note that this inversion uses large spatial regions, and the total flux from a region can only shift according to the assumed spatial pattern, which is based on a priori source estimates. One approach that has been used to deal with artifacts in atmospheric inverse models caused by the use of large model regions is to treat each model grid cell as an individual model region [i.e., *Kaminski et al.*, 1999; *Houweling et al.*, 1999]. This approach eliminates the need for "hard constraints," or features of the trace gas flux that cannot be varied by the inverse model, such as the spatial pattern of the model regions. However, the trade-off associated with the use of a very large number of model regions is that the problem is very poorly constrained by the observations, and in the absence of good observational constraints to the inverse problem the solution can be heavily biased by the a priori estimates. With planned future expansions to the observing network and satellite observations, the use of very small model regions is a logical next step for inverse models; however, on the basis of the currently available observational network, the use of large model regions was chosen for this research to provide strongly data-driven inverse estimates.

4. Inverse $\delta^{13}C$ Estimates

[22] Since observations of $\delta^{13}CH_4$ are only available for six observing stations, the 11 model regions are aggregated to three latitude bands, and the inverse model is used to estimate the net $\delta^{13}CH_4$ isotopic signature from all of the source processes occurring within a model region. This isotopic signature is then used to interpret the likely reasons for important differences between the a priori estimates and the a posteriori estimates both qualitatively and quantitatively (Table 5). The largest change in the isotopic signature of the sources occurs in the southern extratropical region, where the a posteriori isotopic signature of the sources is

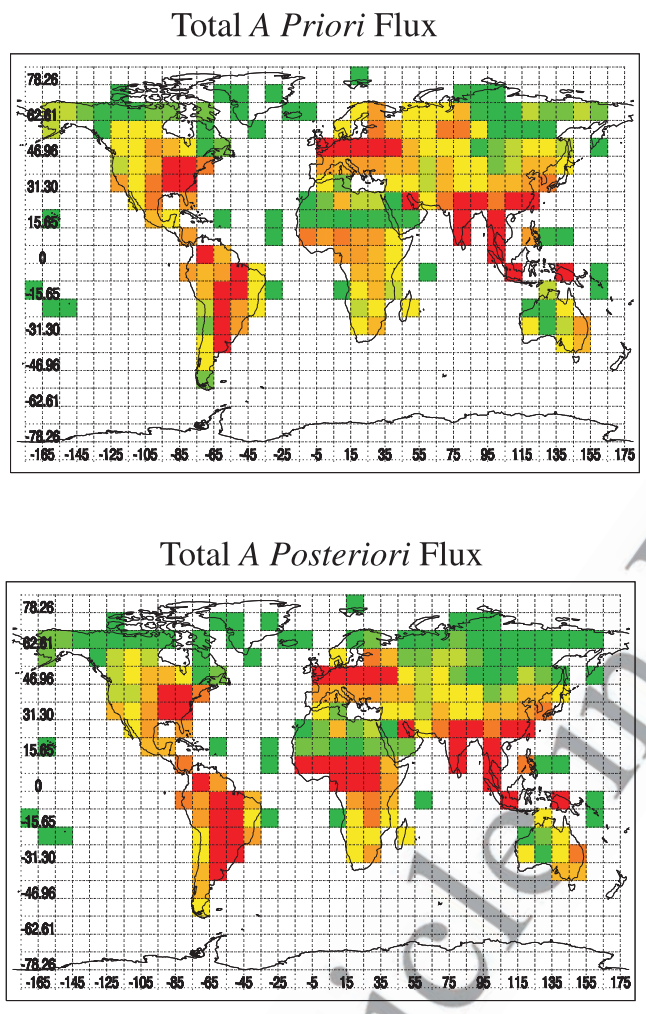

less depleted in ^{13}C than the a priori estimate. Since the total source is increased in this region, the heavier isotopic signature suggests that the sources that are underestimated in the a priori estimates are those that have heavier isotopic signatures, such as biomass burning, although this difference is not large relative to the a posteriori flux increase, so bacterial sources are likely to be underestimated as well.

[23] In the tropics, the estimated isotopic signature is very close to the a priori estimate. It could be argued that poor overall sampling in the tropics may mean that this region is so poorly constrained by the observational data that no new information has been added by the inversion. However, in a regime with only three model regions, if two are reasonably well constrained by the observations, the third is then constrained by mass balance. The CH_4 inversion calls for a large increase in the net source for this region, and the similar inverse isotopic signature implies that a combination of sources that are much more depleted in ^{13}C relative to the atmosphere and those that are enriched relative to the atmosphere must be increased relative to the a priori estimates to maintain the isotope balance. The two isotopically depleted sources that play a major role in the tropics are swamps and ruminant animals. Of these two, the ruminant animal source is relatively well known based on bottom-up inventory techniques, but the swamp source is not, making it the most likely source for a large increase. Biomass burning is very isotopically enriched relative to the background atmosphere, so the isotopic signature of the tropical sources implies large increases in the swamp and biomass burning sources compared to the a priori estimates. This result from the regional inversion is in general agreement with the source-process inversion, which called for very high CH_4 fluxes from swamps and biomass burning which both have large spatial footprints in the tropics [*Mikaloff Fletcher et al.*, 2004].

[24] Finally, in the northern extratropics, the inverse model calls for a similar isotopic signature to the a priori estimates, while the CH_4 inversion calls for a decreased flux. Since the total flux is decreased and the isotopic signature remains similar, either the isotopically heavy and isotopically light sources must both be decreased or sources with a weak isotopic signature relative to the background atmosphere, such as fossil fuels, must be decreased the most. This is a reasonable result for this region since the bulk of the fossil fuel source is emitted in the northern extratropical region.

[25] While this qualitative discussion is useful, a more rigorous source partitioning is highly desirable in order to further understanding of the a posteriori CH_4 fluxes. To this end, the CH_4 sources have been grouped into three major categories based on their isotopic signatures: fossil fuels and

Figure 4. Global distribution of CH_4 flux in Tg CH_4 grid $cell^{-1}$ yr^{-1} averaged over the 1998–1999 inversion time period for (top) a priori estimates and (middle) a posteriori estimates, and (bottom) the difference between the a posteriori estimate and the a priori estimates. This source map was created by distributing the flux estimates from the 11 source regions according to the spatial patterns used to create the basis functions.

t5.1 **Table 5.** Time-Averaged Total ^{13}C Isotopic Signature and CH_4 Flux From Three Latitude Bands (North of 23.5°N, 23.5°N to 15.7°S, and South of 15.7°S) Partitioned Into Bacterial and Biomass Burning Sources[a]

t5.2 Model Region	S0	S1	S2	S3	S4	S5
t5.3			*Northern Extratropics*			
t5.4 ^{13}C isotopic signature	−53.3‰	−53.5‰	−53.2‰	−52.6‰	−54.1‰	−53.0‰
t5.5 Bacterial sources, Tg CH_4/yr	159	124–159	128–163	133–168	107–134	114–149
t5.6 Biomass burning, Tg CH_4/yr	2	−33–−5	−31–−3	−27–1	−41–−13	−34–−6
t5.8			*Tropics*			
t5.9 ^{13}C isotopic signature	−50.3‰	−50.4‰	−48.5‰	−50.1‰	−49.9‰	−51.7‰
t5.10 Bacterial sources, Tg CH_4/yr	122	184–187	164–167	204–207	131–134	191–194
t5.11 Biomass burning, Tg CH_4/yr	48	65–68	81–84	83–85	54–57	58–61
t5.13			*Southern Extratropics*			
t5.14 ^{13}C isotopic signature	−55.8‰	−53.9‰	−51.5‰	−54‰	−53.5‰	−54.9‰
t5.15 Bacterial sources, Tg CH_4/yr	44	76–78	73–75	94–97	56–58	76–79
t5.16 Biomass burning, Tg CH_4/yr	3	13–15	20–23	14–16	9–11	11–13

[a]The isotopic signatures represent the net isotopic signatures from all source processes and were estimated for the scenarios described in Table 2. The total CH_4 source for each latitude band, aggregated from the regional estimates in Table 3, was partitioned into bacterial and biomass burning sources using the estimated net isotopic signature of the total flux, the observed isotopic signatures for each source process, and upper and lower limits of the fossil fuel estimates. Note that the ranges shown in the a posteriori estimates only reflect the t5.17 upper and lower bounds of the fossil fuel range and do not include uncertainty in the inverse estimates.

landfills, biomass burning, and bacterial sources, which include wetlands, ruminant animals, rice paddies, and termites. The mean isotopic signature for each of these source processes was calculated for each latitude band based on a priori estimates. Using mass balance, two equations can be written in terms of three unknowns for each latitude band,

$$S_{tot} = S_{ba} + S_{bb} + S_{ff} \quad (10)$$

$$\delta_{tot}S_{tot} = \delta_{ba}S_{ba} + \delta_{bb}S_{bb} + \delta_{ff}S_{ff}, \quad (11)$$

where S denotes the source strength, δ denotes the isotopic signature, and the subscripts ba, bb, ff, and tot refer to bacterial sources, biomass burning sources, fossil sources, and the total source, respectively. Using the inverse model, the total source and isotopic signatures for each region, S_{tot} and δ_{tot}, have been determined. If one of the source processes could be prescribed, then the other two could be calculated from these equations. The most well known of these three broad categories is the fossil fuel group; therefore, the upper and lower bounds of the *IPCC* [2001] range of estimates for the fossil fuels were applied to these equations, resulting in the high and low estimates of bacterial and biomass burning sources (Table 5). Note that this range does not include uncertainty associated with the inverse estimates or the isotopic signatures of the sources, although the sensitivity of this quantity to changes in the inverse estimates will be explored in the next section.

[26] In the northern extratropics, the bacterial sources are reduced by this partitioning technique relative to the a priori estimates. Interestingly, the source partitioning finds a negative estimate for biomass burning sources, which is clearly a nonphysical result. This suggests that the fossil fuel estimates may be too high, in general agreement with the process-inversion approach, the prescribed sinks may be too low, or the total flux estimates may be too high in this region. The fossil fuel estimates used in this study may be overestimated for Europe; since the spatial distribution of CH_4 used here predates the collapse of the Soviet Union, the spatial distribution of fossil fuels may be overestimated at high northern latitudes. *Dlugokencky et al.* [2003] attributed the decline in the CH_4 growth rate in the early 1990s to the collapse of the Soviet Union which caused changes in the interhemispheric gradient of the observed atmospheric CH_4.

[27] In comparison to the northern extratropics, the tropics and southern extratropics have a small range of estimates due to the relatively small fossil emissions in these areas. Large increases have been estimated for both bacterial and biomass burning sources for these regions. Since ruminant animals are the most well known source and rice cultivation has a more limited spatial extent, wetlands are likely to contribute to a large portion of this bacterial increase. A high wetland source is in general agreement with recent source-process inverse studies [e.g., *Mikaloff Fletcher et al.*, 2004; *Hein et al.*, 1997]. In addition, some recent wetland models have estimated a large spatial extent of wetlands [*Kaplan*, 2001] and very high CH_4 fluxes [*Walter*, 1998] compared with wetland inventory approaches. *Chen* [2004] found emissions from biomass burning and bacterial sources with strong spatial footprints in the tropics that were close to the high end of the range of bottom-up source estimates, but are still lower than the inverse estimates presented here.

5. Interannual Variability

[28] One of the key advantages of inverse modeling is the ability to diagnose observed anomalies in the atmospheric mixing ratio of a trace gas when clear, quantitative process-level observations of the source phenomenon responsible are not available. The annual means for 1998 and 1999 can be used to attempt to attribute the 1998 CH_4 growth rate anomaly [*Dlugokencky et al.*, 2001] to a region or source process. Since the model requires 3 months of spin-up time, and the $\delta^{13}CH_4$ observations did not begin until 1998, the inverse estimates for 1998 are only for April–December.

t6.1 **Table 6.** Mean A Priori and Inverse Estimates of CH_4 Flux From the 11 Inverse Model Regions for April to December 1998 and All of 1999[a]

t6.2 Model Region	A priori Estimates April–Dec. Mean, Tg CH_4/yr	A Posteriori (S1) 1998 April–Dec. Mean, Tg CH_4/yr	A Priori Estimates Annual Mean, Tg CH_4/yr	A Posteriori (S1) 1999 Annual Mean, Tg CH_4/yr
t6.3 Boreal North America	24 ± 16	23 ± 6	19 ± 16	12 ± 4
t6.4 Boreal Eurasia	48 ± 28	26 ± 9	39 ± 28	8 ± 7
t6.5 Temperate North America	58 ± 13	62 ± 9	58 ± 13	49 ± 8
t6.6 Europe	71 ± 15	60 ± 8	68 ± 15	76 ± 8
t6.7 Temperate Eurasia	103 ± 42	112 ± 11	94 ± 42	87 ± 10
t6.8 Tropical South America	53 ± 25	83 ± 18	53 ± 25	67 ± 15
t6.9 Northern Africa	47 ± 21	80 ± 16	48 ± 21	80 ± 17
t6.10 Tropical Asia	76 ± 38	117 ± 10	76 ± 38	110 ± 9
t6.11 Southern Africa	8 ± 3	9 ± 2	9 ± 3	10 ± 3
t6.12 Temperate South America	36 ± 20	64 ± 14	37 ± 20	77 ± 14
t6.13 Australia	13 ± 4	19 ± 4	13 ± 4	16 ± 4
t6.14 **Global**	**537 ± 78**	**651 ± 29**	**515 ± 78**	**584 ± 28**

t6.15 [a]Note that the a priori source estimates do not include interannual variability. The differing a priori sources from 1998 to 1999 reflect the seasonality of the sources since the two time-averaged values include different months.

The differences in the 1998 and 1999 a priori estimates (Tables 6 and 7) reflect this seasonal bias, and there is no interannual variability in the a priori estimates.

[29] 1998 was characterized by a transition from a very strong El Niño, lasting until early May, to a La Niña, beginning in July [*Bell et al.*, 1999]. Model simulations of atmospheric CH_4 mixing ratios have shown that meteorology can have an important effect on interannual variations in atmospheric CH_4 [*Warwick et al.*, 2002]. However, interannual variability due to changes in meteorology is accounted for because the model is driven by assimilated meteorological fields corresponding to the model year rather than repeating a single year of meteorology.

[30] The bulk of the wetlands in the northern extratropical latitude band occur in the boreal North America and boreal Eurasia model regions. The inverse emissions estimates are larger for these regions in 1998 than 1999 (Table 6). In addition, the estimated isotopic signature is much more depleted in ^{13}C in 1998 than 1999 (Table 7), leading to a large decrease in the calculated bacterial sources from 1998 to 1999. Since ruminant animal sources do not vary greatly on interannual timescales and termites and rice paddies are only minor contributors to the budget in these regions, this change is attributable to wetlands in general agreement with the conclusions of *Dlugokencky et al.* [2001] and the source process inversion [*Mikaloff Fletcher et al.*, 2004]. The year 1998 was marked by elevated temperatures in boreal North America and Eurasia from June to August [*Bell et al.*, 1999] and elevated precipitation in some high northern latitude regions from April to September [*Curtis et al.*, 2001], which could explain elevated wetland emissions from high-latitude wetlands [*Dlugokencky et al.*, 2001]. Although there is a large range in the source partitioning for this region due to the uncertainty in the fossil sources, since none of the fossil sources is known to have such large variability on these timescales, the interannual change is expected to be robust.

[31] In the tropics and southern extratropics, the 1998–1999 variability in the a posteriori CH_4 flux and $\delta^{13}C$ isotopic signature is much smaller than in the northern extratropics. Owing to the relatively small variability and

t7.1 **Table 7.** Mean A Priori and Inverse Estimates of the CH_4 Sources for April to December 1998 and All of 1999 Partitioned Using the Isotopic Signatures of the Sources and the Upper and Lower Bounds of Estimated Fossil Fuel Emissions[a]

t7.2 Model Region	A Priori Estimates April–Dec. Mean, Tg CH_4/yr	A Posteriori (S1) 1998 April–Dec. Mean, Tg CH_4/yr	A Priori Estimates Annual Mean, Tg CH_4/yr	A Posteriori (S1) 1999 Annual Mean, Tg CH_4/yr
t7.3		*Northern Extratropics*		
t7.4 ^{13}C Isotopic signature	−53.7‰	−56.2‰	−53.0‰	−51.8‰
t7.5 Bacterial sources, Tg CH_4/yr	181	162–197	148	99–134
t7.6 Biomass burning, Tg CH_4/yr	2	−46–−18	2	−25–3
t7.8		*Tropics*		
t7.9 ^{13}C isotopic signature	−50.6‰	−50.2‰	−50.2‰	−50.6‰
t7.10 Bacterial sources, Tg CH_4/yr	137	193–195	122	178–181
t7.11 Biomass burning, Tg CH_4/yr	52	68–71	48	64–66
t7.13		*Southern Extratropics*		
t7.14 ^{13}C isotopic signature	−55.8‰	−52.3‰	−56.0‰	−55.1‰
t7.15 Bacterial sources, Tg CH_4/yr	52	70–72	48	80–82
t7.16 Biomass burning, Tg CH_4/yr	3	17–19	2	11–13

t7.17 [a]Note that the a priori source estimates do not include interannual variability. The differing a priori sources from 1998 to 1999 reflect the seasonality of the sources since the two time-averaged values include different months.

the poor observational coverage in these regions, these results must be interpreted with caution. The largest variations in the tropics and southern extratropics over this time period were a moderate decrease in CH_4 flux from tropical South America between 1998 and 1999 and a smaller increase in temperate South America. However, owing to the limited observational constraints on these regions, the partitioning between these regions may not be robust. Since the a posteriori tropical isotopic source signature changes very little from 1998 to 1999, the elevated South American flux estimates in 1998 would most likely be due to an increase in both biomass burning and wetland sources (Table 7). Conversely, in the southern extratropics, while there is little change in the CH_4 flux estimates, the isotopic signatures suggest that that there may have been a small increase in bacterial sources and a decrease in biomass burning in 1999.

6. Sensitivity of the Results

[32] The inverse model was tested for sensitivity to changes in the model, as summarized in Table 3. The first scenario, S0, is simply the a priori CH_4 budget, and S1 is the standard inverse model scenario. If not otherwise specified, discussion of the a posteriori results in this paper refers to S1. S2 applies a more recent measurement of the OH Kinetic Isotope Effect (KIE) [*Saueressig et al.*, 2001]. S3 and S4 test the upper and lower limits of the magnitude of the OH sink, based on the uncertainty estimates of *Spivakovsky et al.* [2000]. Finally, in S5 the model sensitivity to initial conditions is tested by initializing the inverse model to hemispheric mean CH_4 mixing ratios and $\delta^{13}CH_4$, rather than the model simulated three-dimensional CH_4 and $\delta^{13}CH_4$ fields used in S1 through S4. The inverse estimates for these scenarios are shown in Tables 4 and 5.

[33] In general, the results for the 11 regions CH_4 inversion show very little variation between inverse scenarios. Changing the KIE (S2) perturbs the CH_4 estimates very slightly in comparison to S1, the base scenario. This perturbation is due to the iterative process that allows the inverse estimate of the isotopic signature to add constraints to the initial CH_4 inversion. As expected due to the relatively small effect of including this iterative process on the CH_4 inversion, the CH_4 flux estimates are relatively insensitive to this change.

[34] Using the upper and lower bounds of the OH fields based on their estimated uncertainty [*Spivakovsky et al.*, 2000] in S3 and S4 has a much greater impact on the resulting CH_4 estimates. Changes in the estimated CH_4 flux with changes in the OH field are less than or close to the error estimates for the northern extratropical regions. In the tropical regions of South America, Northern Africa, and Asia, the effect of changes to the OH field is much greater due to the larger concentration of OH in the tropics. The difference between the base scenario and the lower limit of the OH uncertainty exceeds the error estimate on the inverse calculations for these regions. The OH fields in S1 have been scaled up from the original OH fields to match the *IPCC* [2001] estimate for CH_4 uptake, but the uncertainty limit changes to the OH fields were applied to the original values, so the upper and lower limit OH field scenarios are not symmetrical around the base scenario, S1. In the southern extratropical regions of Southern Africa and Australia, the perturbations to the OH field have relatively little impact on the resulting CH_4 flux estimates, which are fairly similar to the a priori estimates. The largest changes occur in temperate South America. In this region, S1 estimates a large increase in CH_4 flux relative to the a priori estimate, but in the lower limit of the OH field estimates, this increase is smaller than the uncertainty estimates for the inverse model. Therefore this result may not be robust in the limit of low OH. Finally, changes in the initial conditions have little effect on the CH_4 flux estimates.

[35] The a posteriori isotopic signatures for the five inverse scenarios vary by up to 3.4‰, whereas the variations between the a priori and a posteriori isotopic signatures (S0 and S1) are between zero and 1.9‰ (Table 5). This implies that qualitative interpretation of these results based on relative changes between a priori and a posteriori estimates should be treated with caution since the variations with change in model parameters are often larger than these differences.

[36] One issue of concern about the sensitivity tests for the isotopic signature inversion is that changes in the initial conditions (S5) have a surprisingly large influence on the inverse estimates. Recent work has shown that the isotopic ratio takes much longer to reach steady state than CH_4 [*Tans*, 1997; *Lassey et al.*, 2000]. The initial conditions for S5 assume a uniform mixing ratio and atmospheric $\delta^{13}CH_4$ for each hemisphere for all vertical levels based on the observed hemispheric mean at the surface. In this very poor representation of the atmosphere, it is likely that the 3-month spin-up time is not sufficient for surface fluxes to establish vertical and latitudinal gradients that reflect the atmosphere. However, the current initial conditions, which are based on a preliminary inverse run, should be close enough to the real atmosphere to avoid this problem.

[37] Despite these variations in the net isotopic signature of the sources, the quantitative source partitioning estimates are fairly robust with respect to these inverse scenarios (Table 5), providing strong conclusions for the tropics and southern extratropics. In the tropics and southern extratropics, all of the inverse scenarios call for increases in both the bacterial and biomass burning sources, although in the low OH limit, these increases are fairly small. Owing to the limited contributions from fossil fuels in these regions, the source partitioning approach provides a very good constraint for these regions.

[38] Finally, the partitioning of CH_4 sources into source processes using ^{13}C has been shown to be sensitive to errors in the observed isotopic signature of the sources [*Miller et al.*, 2002]. The effect of moderate errors in the source signatures used to partition the sources is shown by adjusting each of the isotopic signatures used to partition the sources in turn by ±2 in Table 8. The source partitioning is somewhat sensitive to these fairly small changes in the isotopic signatures used, especially in the case of the bacterial sources errors in the isotopic signature. For example, a 4‰ change in the bacterial isotopic signature results in a shift of 19 Tg CH_4 from bacterial to biomass

t8.1 **Table 8.** Sensitivity of the Partitioning of the Sources Into Source Processes to the Isotopic Signature of Source Processes[a]

t8.2 Model Region	S1	δ_{ba} − 2‰	δ_{ba} + 2‰	δ_{bb} − 2‰	δ_{bb} + 2‰	δ_{ff} − 2‰	δ_{ff} + 2‰
t8.3			*Northern Extratropics*				
t8.4 Bacterial sources	124–159	117–151	131–198	126–160	122–159	115–154	133–165
t8.5 Biomass burning	−33–−5	−26–+3	−40–−15	−35–−6	−31–−5	−25–0.1	−42–−11
t8.7			*Tropics*				
t8.8 Bacterial sources	184–187	174–177	195–198	180–183	188–190	183–187	185–188
t8.9 Biomass burning	65–68	75–78	54–57	69–72	62–64	66–69	65–68
t8.11			*Southern Extratropics*				
t8.12 Bacterial sources	76–78	72–74	81–83	75–77	77–79	76–78	77–79
t8.13 Biomass burning	13–15	17–20	9–11	14–16	13–15	14–16	13–15

[a]The first column shows the a posteriori sources partitioned into bacterial and biomass burning sources using the isotopic signatures shown in Table 1. Subsequent columns illustrate the effect on the source partitioning of reducing or increasing the bacterial isotopic t8.14 signature (δ_{ba}), the biomass burning isotopic signature (δ_{bb}), or the fossil isotopic signature (δ_{ff}) by 2‰.

burning sources in the tropics (Table 8, columns 2 and 3). However, most of the broad qualitative conclusions of this work still apply.

[39] In addition to the likely sources of error that have been tested in this section, the transport model chosen is likely to play an important role in the inverse estimates. For example, the preferred source scenario of *Fung et al.* [1991] was selected by the authors in part because forward model simulations matched the observations so well, but forward simulations of these sources using TM3 result in an overestimate of the interhemispheric gradient [*Mikaloff Fletcher*, 2003]. While most inverse studies of CH_4 have used TM3 or TM2, an earlier version [e.g., *Hein et al.*, 1997; *Houweling et al.*, 1999], the recent work of *Chen* [2004] used the Model of Atmospheric Transport and Chemistry (MATCH). There are many similarities between the overall conclusions of *Chen* [2004] and this work. Both inverse studies estimate relatively high fluxes from biomass burning and bacterial sources in the tropics, suggest decreases in fossil emissions, and attribute the bulk of the 1998 CH_4 anomaly to wetlands. However, there are important quantitative differences between the inverse flux estimates. These differences cannot be attributed to the transport model alone because there were many other methodological differences between these two studies, including the inverse methodology, the types of data used, and the representation of the sinks.

[40] Finally, the inverse methodology may lead to error. The inverse method used in this study also incorporates only 1 month of model transport, and errors in the a posteriori estimates for a given model transport are likely to be propagated to future months. While the CH_4 inversion is expected to be subject to less aggregation error than source process inversions of CH_4 [e.g., *Mikaloff Fletcher et al.*, 2004; *Hein et al.*, 1997], the 11 regions chosen here are still relatively large and are expected to introduce some aggregation error. Owing to the larger regions used for the estimates of the isotopic signatures, aggregation error is likely to be more important for these estimates.

7. A Posteriori Atmospheric CH_4 Mixing Ratios and $\delta^{13}CH_4$

[41] Finally, the ability of the inverse estimates to reproduce the atmospheric observations of CH_4 and $\delta^{13}CH_4$ is tested. As expected, owing to the observational constraints to the inverse model, the a posteriori CH_4 mixing ratio and atmospheric $\delta^{13}CH_4$ are a far better match to the atmospheric observations than the forward simulation of a priori sources (Figures 1, 5, and 6). The inverse estimates reproduce the observed latitudinal gradient of atmospheric CH_4 very well, correcting the overestimate of this gradient that results from the a priori sources (Figure 1, top). The two stations that have unusually high CH_4 mixing ratios for their latitude, Black Sea, Romania, and Cape Rama, India, are not well matched by the inverse estimates due to the strong local source signal for these stations and the higher uncertainty weighting of stations sampling continental air, as discussed by *Mikaloff Fletcher et al.* [2004]. The inverse estimates also match the latitudinal gradient of the $\delta^{13}CH_4$ observations very well, with the model falling within the standard deviation of the observations, based on the standard deviation of the individual observations from the mean, for all of the stations (Figure 1, bottom).

[42] In general, monthly mean inverse model results at the observing stations are also in good agreement with the observations for both CH_4 and $\delta^{13}CH_4$. The observed atmospheric CH_4 mixing ratios and $\delta^{13}CH_4$ are compared with the simulated CH_4 mixing ratios and $\delta^{13}CH_4$ based on the a priori and a posteriori estimates (Figures 5 and 6) for the sampling sites with observations of both quantities, described in Table 8. While the a posteriori $\delta^{13}CH_4$ is generally in good agreement with the observations, it does not capture the full seasonal variability at BRW or the SPO trough in early 1999. In the case of BRW, this may be due to the fact that this site is strongly influenced by CH_4 fluxes from boreal North America and Eurasia, which are expected to have a larger relative contribution of wetland CH_4 than the other regions included in the Northern Extratropical latitude band. Therefore the a posteriori isotopic signature which was estimated for an aggregate of all of the northern extratropical regions may not effectively represent conditions at this station. Owing to the dearth of CH_4 sources at high latitudes, the winter trough at SPO is also not well matched by the a posteriori inverse estimates. This anomalous feature may be due to long-term transport of anomalously high wetland emis-

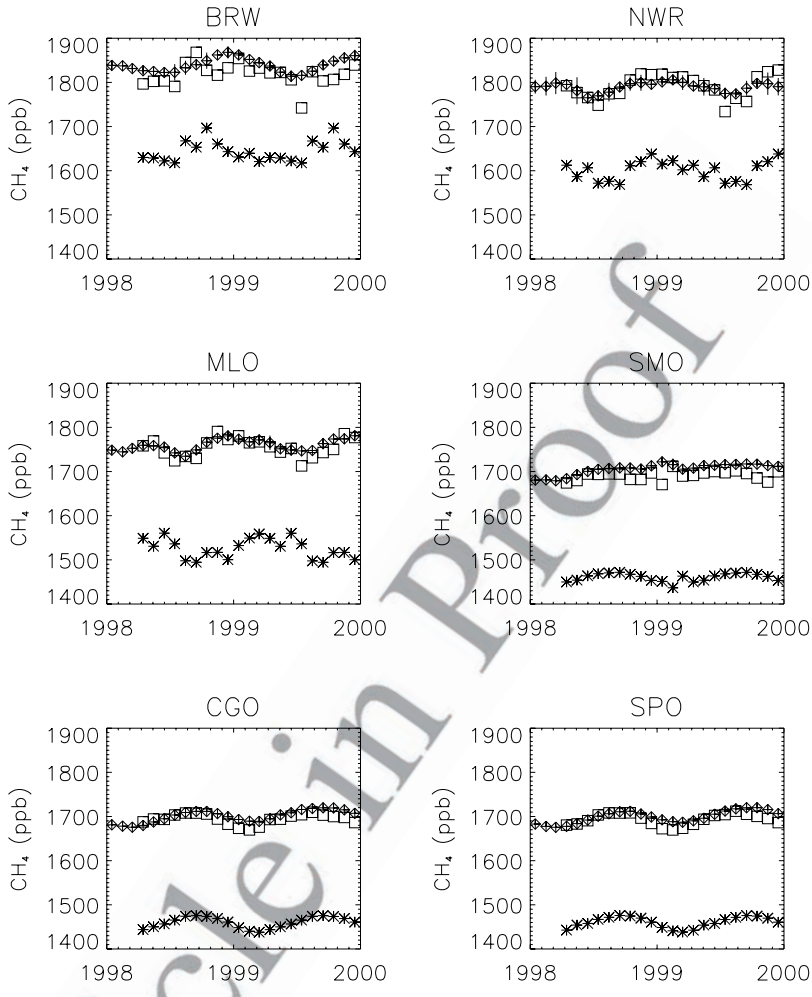

Figure 5. Comparison between the monthly mean CH_4 measurement record at six observing stations (diamonds), model simulation based on a priori sources (asterisks), and the model simulation based on the a posteriori sources (squares). The observing stations are shown in Table 2. Error bars on the measurements represent the standard deviation of the individual observations from the smoothed curve.

sions at high southern latitudes at the end of 1998 (J. White, personal communication, 2002).

[43] The a posteriori atmospheric $\delta^{13}CH_4$ has also been compared with National Institute of Water and Atmospheric Research (NIWA) observations of $\delta^{13}CH_4$ at Baring Head, New Zealand, and Scott Base, Antarctica [*Lowe et al.*, 1994], which were not used to constrain the inverse model (Figure 7). The modeled $\delta^{13}CH_4$ is slightly isotopically lighter than the observed values at the NIWA stations, while matching the observations at the CMDL stations. *Miller et al.* [2002] suggested that the NIWA observations might be about 0.1‰ lighter than the CMDL databased on comparisons between observations at Cape Grim and Baring Head, since these two stations are at similar latitudes. However, Figure 7 implies that a source distribution which matches the observations of CH_4 could account for this offset or even a small offset in the opposite direction. Without careful measurement intercomparisons, it is not clear whether the offsets shown in Figure 7 are due to errors in the inverse estimates or offsets between networks.

8. Conclusions

[44] A novel, iterative inverse approach was presented estimating the geographical distribution of CH_4 flux and the $\delta^{13}CH_4$ isotopic signature of the CH_4 flux that is optimally consistent with the observed spatiotemporal atmospheric CH_4 and $\delta^{13}CH_4$ distributions. Relative to most bottom-up source estimates, the atmospheric observation call for a large decrease in the NH CH_4 source estimate, a large increase in CH_4 sources in the tropics, and a smaller increase in CH_4 flux from the southern extratropics. This result is robust and in excellent agreement with previous inverse modeling studies of CH_4 [e.g., *Hein et al.*, 1997; *Houweling et al.*, 1999; *Chen*, 2004; *Mikaloff Fletcher et al.*, 2004]. The inverse model yields reduction in the uncertainty of the a priori estimates, especially in NH regions.

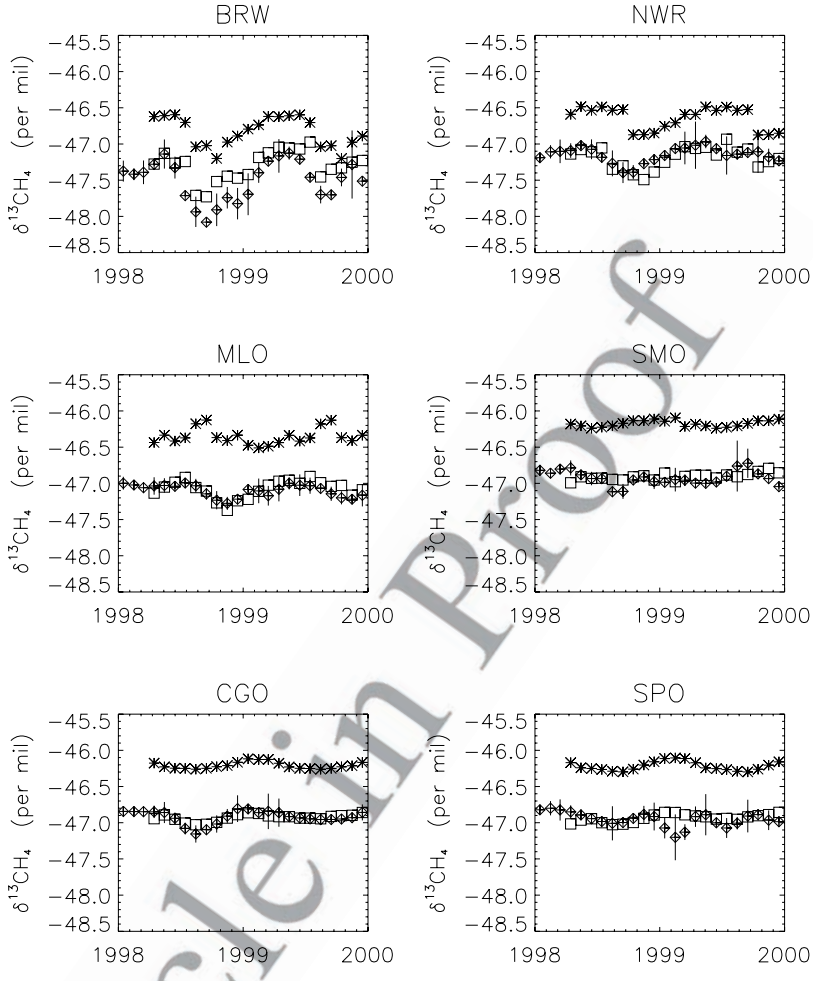

Figure 6. Comparison between the monthly mean $\delta^{13}CH_4$ measurement record at six observing stations (diamonds), model simulation based on a priori sources (asterisks), and the model simulation based on the a posteriori sources (squares). Error bars on the measurements represent the standard deviation of the individual observations from the smoothed curve.

[45] The a posteriori CH_4 fluxes were partitioned into bacterial and biomass burning sources using inverse estimates of the net isotopic signature of the flux and upper and lower bound estimates of the fossil fuel and landfill fluxes. This partitioning technique implies that the estimates for fossil fuels in the northern extratropics may be inconsistent with atmospheric observations of CH_4 and $\delta^{13}CH_4$. In the tropics and southern extratropics, the source increase in total CH_4 flux relative to the a priori estimates was attributed to a large increase in both biomass burning and swamps.

[46] The time-dependent inverse estimates of the CH_4 flux and its isotopic ratios provide new insight into the causes behind the 1998 growth rate anomaly. The variations between 1998 and 1999 support the hypothesis of *Dlugokencky et al.* [2001] that wetlands were primarily responsible for the anomalous growth rate in 1998, although increases in biomass burning are also estimated for 1998 over 1999.

[47] The total CH_4 flux estimate and the partitioning of the source between bacterial and biomass burning sources was generally robust with respect to variations in the KIE oxidation of CH_4 by OH, the upper bound of the OH fields, the choice of transport year, and model initialization. However, the source partitioning was somewhat sensitive to modest changes in the isotopic signatures of the sources.

[48] The overall agreement in the major conclusions of this inverse approach and an earlier source-process inversion [*Mikaloff Fletcher et al.*, 2004] suggests that these results are robust with respect to the model region selection and the methodology used to incorporate constraints from the $\delta^{13}CH_4$. However, there are several significant ongoing limitations to these inverse estimates. Since this inverse technique only carries 1 month of model transport at a time, the monthly variations in the inverse estimates are "noisy" and the potential to draw robust conclusions from the time series is limited. Owing to the nonlinearity of the problem, any errors associated with the CH_4 flux estimates will be propagated to the estimates of the isotopic signatures. In addition, error in model transport could introduce significant uncertainties. Finally, even with the addition of isotopic

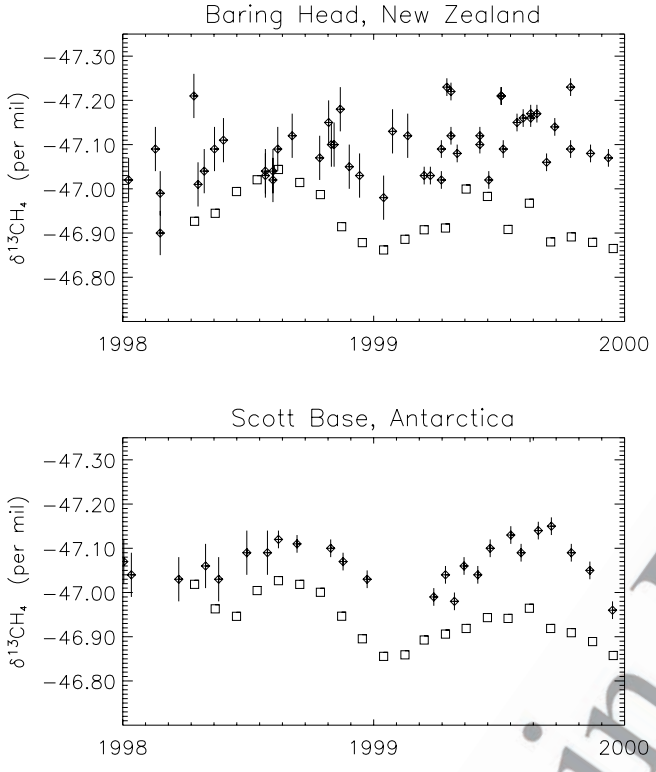

Figure 7. Comparison between the $\delta^{13}CH_4$ measurement (diamonds) and the model simulation based on the a posteriori sources (squares) for two NIWA observing stations: Baring Head, New Zealand and Scott Base, Antarctica [*Lowe et al.*, 1994].

observations, the inverse calculation remains data limited and expansions to the observing network are needed as well.

[49] **Acknowledgments.** This paper has benefited greatly from thoughtful discussions and comments from Ed Dlugokencky, Jim White, and Scott Denning. We would like to thank the scientists responsible for the observations that made this work possible, including all of the contributors to the Cooperative Air Sampling Network and the Carbon Cycle Greenhouse Gases Group at NOAA. We are especially grateful to Ed Dlugokencky for his work on methane measurements and interpretation of trends in methane observations, Jim White and INSTARR for the measurements of $^{13}C/^{12}C$ isotopic ratios in CH_4, and Ken Masarie for his work on the GLOBALVIEW data product. The authors also acknowledge Dave Lowe, Gordon Brailsford, and Ross Martin for the $\delta^{13}CH_4$ observations at Baring Head, New Zealand, and Scott Base, Antarctica. S. F., P. T., L. B., and J. M. acknowledge the NOAA Office of Oceanic and Atmospheric Research for support. S. F. also acknowledges CIRES for support through the Graduate Research Fellowship program and the Biosphere Atmosphere Stable Isotope Network (BASIN) for travel funding that facilitated the development of this work. This research has also been presented in S. F.'s doctoral dissertation at the University of Colorado, Boulder, Boulder, Colorado, USA, 2003.

References

Aselmann, I., and P. J. Crutzen (1989), Global distribution of natural freshwater wetlands and rice paddies, their net primary productivity, seasonality, and possible methane emissions, *J. Atmos. Chem.*, *8*, 307–358.

Bell, G. D., M. S. Halpert, C. F. Ropelewski, V. E. Kousky, A. V. Douglas, R. C. Schnell, and M. E. Gelman (1999), Climate assessment for 1998, *Bull. Am. Meteorol. Soc.*, *80*, S1–S48.

Bergamaschi, P., M. Bräunlich, T. Marik, and C. A. M. Brenninkmeijer (2000), Measurements of the carbon and hydrogen isotopes of atmospheric methane at Izaña, Tenerife: Seasonal cycles and synoptic-scale variations, *J. Geophys. Res.*, *105*, 14,531–14,546.

Bingemer, H. G., and P. J. Crutzen (1987), The production of methane from solid wastes, *J. Geophys. Res.*, *92*, 2181–2187.

Brenninkmeijer, C. A. M., D. C. Lowe, M. R. Manning, R. J. Sparks, and P. F. J. van Velthoven (1995), The ^{13}C, ^{14}C, and ^{18}O isotopic composition of CO, CH_4, and CO_2 in the higher southern latitudes lower stratosphere, *J. Geophys. Res.*, *100*, 26,163–26,172.

Bruhwiler, L., P. Tans, and M. Ramonet (2000), A time-dependent assimilation and source retrieval technique for atmospheric tracers, in *Inverse Methods in Global Biogeochemical Cycles*, *Geophys. Monogr. Ser.*, vol. 114, edited by P. Kasibhatla et al., pp. 265–277, AGU, Washington, D. C.

Cantrell, C. A., R. E. Shetter, A. H. McDaniel, J. G. Calvert, J. A. Davidson, D. C. Lowe, S. C. Tyler, R. J. Cicerone, and J. P. Greenberg (1990), Carbon kinetic isotope effect in the oxidation of methane by the hydroxyl radical, *J. Geophys. Res.*, *95*, 22,455–22,462.

Chen, Y.-H. (2004), Estimation of methane and carbon dioxide surface fluxes using a 3-D global atmospheric chemical transport model, Ph.D. thesis, Mass. Inst. of Technol., Cambridge, Mass.

Cicerone, R. J., and R. S. Oremland (1988), Biogeochemical aspects of atmospheric methane, *Global Biogeochem. Cycles*, *2*, 299–327.

Craig, H. (1953), The geochemistry of stable carbon isotopes, *Geochim. Cosmochim. Acta*, *3*, 53–92.

Curtis, S., R. Adler, G. Huffman, E. Nelkin, and D. Bolvin (2001), Evolution of tropical and extratropical precipitation anomalies during the 1997–1999 ENSO Cycle, *Int. J. Climatol.*, *21*, 961–967.

Dlugokencky, E. J., B. P. Walter, K. A. Masarie, P. M. Lang, and E. S. Kasischke (2001), Measurements of an anomalous global methane increase during 1998, *Geophys. Res. Lett.*, *28*, 499–502.

Dlugokencky, E. J., S. Houweling, L. Bruhwiler, K. A. Masarie, P. M. Lang, J. B. Miller, and P. P. Tans (2003), Atmospheric methane levels off: Temporary pause or a new steady state?, *Geophys. Res. Lett.*, *30*(19), 1992, doi:1029/2003GL017475.

Fung, I., J. John, J. Lerner, E. Matthews, M. Prather, L. P. Steele, and P. J. Fraser (1991), Three-dimensional model synthesis of the global methane cycle, *J. Geophys. Res.*, *96*, 13,033–13,065.

Heimann, M., and S. Körner (2003), The Global Atmospheric Tracer Model TM3 model description and user's manual, technical report, Max-Planck-Inst. für Biogeochem., Jena, Germany.

Hein, R., P. J. Crutzen, and M. Heimann (1997), An inverse modeling approach to investigate the global atmospheric methane cycle, *Global Biogeochem. Cycles*, *11*, 43–76.

Houweling, S., T. Kaminski, F. Dentener, J. Lelieveld, and M. Heimann (1999), Inverse modeling of methane sources and sinks using the adjoint of a global transport model, *J. Geophys. Res.*, *104*, 26,137–26,160.

Intergovernmental Panel on Climate Change (2001), *Climate Change 2001: The Scientific Basis*, edited by J. T. Houghton et al., Cambridge Univ. Press, New York.

Kaminski, T., M. Heimann, and R. Giering (1999), A coarse grid three-dimensional inverse model of the atmospheric transport: 1. Adjoint model and Jacobian matrix, *J. Geophys. Res.*, *104*, 18,535–18,553.

Kaplan, J. O. (2001), Wetlands at the Last Glacial Maximum: Distribution and methane emissions, *Geophys. Res. Lett.*, *29*, 6–10.

Lassey, K. R., D. C. Lowe, and M. R. Manning (2000), The trend in atmospheric methane $\delta^{13}C$ and implications for isotopic constraints on the global methane budget, *Global Biogeochem. Cycles*, *14*, 41–49.

Lelieveld, J., P. J. Crutzen, and F. S. Dentener (1998), Changing concentration, lifetime, and climate forcing of atmospheric methane, *Tellus*, *Ser. B*, *50*, 128–150.

Levine, J. S., W. R. Coffer III, and J. P. Pinto (2000), Biomass burning, in *Atmospheric Methane: Its Role in Global Environment*, edited by M. A. K. Khalil, Springer-Verlag, New York.

Lowe, D. C., C. A. M. Brenninkmeijer, G. W. Brailsford, K. Lassey, A. J. Gomez, and E. G. Nisbet (1994), Concentration and ^{13}C records of atmospheric methane in New Zealand and Antarctica: Evidence for changes in methane sources, *J. Geophys. Res.*, *99*, 16,913–16,925.

Matthews, E., and I. Fung (1987), Methane emissions from natural wetlands: Global distribution, area, and environmental characteristics of sources, *Global Biogeochem. Cycles*, *1*, 61–86.

Mikaloff Fletcher, S. E. M. (2003), Constraining methane flux estimates using observations of atmospheric methane and $^{13}C/^{12}C$ isotopic ratios in methane, Ph.D. thesis, Univ. of Colo., Boulder.

Mikaloff Fletcher, S. E., P. P. Tans, L. M. Bruhwiler, J. B. Miller, and M. Heimann (2004), CH_4 sources estimated from atmospheric observations of CH_4 and its $^{13}C/^{12}C$ isotopic ratios: 1. Inverse modeling of source processes constraining CH_4 source estimates with atmospheric observa-

tions of CH_4 and $^{13}C/^{12}C$ isotopic ratios in CH_4 in an inverse model, *Global Biogeochem. Cycles*, doi:10.1029/2004GB002223, in press.
Miller, J. B., K. A. Mack, R. Dissly, J. W. C. White, E. J. Dlugokencky, and P. P. Tans (2002), Development of analytical methods and measurements of $^{13}C/^{12}C$ in atmospheric CH_4 from the NOAA/CMDL global air sampling network, *J. Geophys. Res.*, *107*(D13), 4178, doi:10.1029/2001JD000630.
National Oceanic and Atmospheric Administration, (2001), GLOBALVIEW-CH_4: Cooperative Atmospheric Data Integration Project- Methane [CD-ROM], report, Clim. Monit. and Diag. Lab., Boulder, Colo. (Also available at ftp.cmdl.noaa.gov, Path: ccg/ch4/GLOBALVIEW)
Olivier, J. G. J., A. F. Bouwman, C. W. M. van der Maas, J. M. Berdowski, C. Veldt, J. P. J. Bloos, A. J. H. Visschedijk, P. J. Zandveld, and J. L. Haverlag (1996), Description of Edgar Version 2.0: A set of global emission inventories of greenhouse gases and ozone-depleting substances for all anthropogenic and most natural sources on a per country basis and on 1×1 grid, report, Natl. Inst. of Public Health and the Environ., Bilthoven, Netherlands.
Petit, J. R., et al. (1999), Climate and atmospheric history of the past 42,0000 years from the Vostok ice core, Antarctica, *Nature*, *399*, 429–436.
Quay, P., J. Stutsman, D. Wilbur, A. Snover, E. Dlugokencky, and T. Brown (1999), The isotopic composition of atmospheric methane, *Global Biogeochem. Cycles*, *13*, 445–461.
Sanderson, M. G. (1996), Biomass of termites and their emissions of methane and carbon dioxide: A global database, *Global Biogeochem. Cycles*, *10*, 543–557.
Saueressig, G., J. N. Crowley, P. Bergamaschi, C. Brühl, C. A. M. Brenninkmeijer, and H. Fischer (2001), Carbon 13 and D kinetic isotope effects in the reactions of CH_4 with O (^1D) and OH: New laboratory measurements and their implications for the isotopic composition of stratospheric methane, *J. Geophys. Res.*, *106*, 23,127–23,138.
Spivakovsky, C. M., et al. (2000), Three-dimensional climatological distribution of tropospheric OH: Update and evaluation, *J. Geophys. Res.*, *105*, 8931–8980.
Tans, P. P. (1997), A note on isotopic ratios and the global atmospheric methane budget, *Global. Biogeochem. Cycles*, *11*, 77–81.
Tyler, S. C., P. M. Crill, and G. W. Brailsford (1994), $^{13}C/^{12}C$ fractionation of methane during oxidation in a temperate forested soil, *Geochim. Cosmochim. Acta*, *58*, 1625–1633.
Walter, B. (1998), Development of a process-based model to derive methane emissions from natural wetlands for climate studies, Ph.D. thesis, Univ. Hamburg, Germany.
Warwick, N. J., S. Bekki, K. S. Law, E. G. Nisbet, and J. A. Pyle (2002), The impact of meteorology on the interannual growth rate of atmospheric methane, *Geophys. Res. Lett.*, *29*, 1947–1951.
Whiticar, M. (1993), Stable isotopes in global budgets, in *Atmospheric Methane—Sources, Sinks, and Role in Environmental Change*, *NATO ASI Ser.: Global Environ. Change*, vol. 1, edited by M. A. K. Khalil, Springer-Verlag, New York.

L. Bruhwiler, J. Miller, and P. Tans, NOAA CMDL, R/CMDL-1, 325 Broadway, Boulder, CO 80305, USA. (lori.bruhwiler@.noaa.gov; john.b.miller@cmdl.noaa.gov; pieter.tans@noaa.gov)
M. Heimann, Max-Planck-Institut für Biogeochemie, Postfach 10064, D-0771 Jena, Germany. (martin.heimann@bgc-jena.mpg.de)
S. Mikaloff Fletcher, Department of Atmospheric and Oceanic Sciences, University of California, Los Angeles, 5839 Schlicter Hall, Los Angeles, CA 90024, USA. (fletcher@igpp.ucla.edu)